镁合金真空电子束深熔焊接及焊缝成形数值模拟

罗　怡[1,2,3]，　刘金合[1]，　叶　宏[3]，　申　彬[3]
（1. 西北工业大学 材料学院，西安　710072；
2. 江苏科技大学 先进焊接技术省级重点实验室，江苏 镇江　212003；
3. 重庆理工大学 材料科学与工程学院，重庆　400050）

摘　要：对 10 mm AZ61镁合金板材进行了真空电子束深熔焊接数值模拟研究. 考虑到焊接过程中高温金属蒸气等离子体的热效应及真空电子束焊接“匙孔”深熔热效应特征，建立了高斯面热源与双椭球体热源复合的移动热源模型，采用数值模拟的方法研究了镁合金真空电子束焊接温度循环特征及不同焊接工艺对焊缝成形的影响. 结果表明，建立的复合热源模型能够获得电子束深熔焊接的效果，并可模拟不同焊接工艺下的温度场分布与电子束热源作用下的焊缝成形，这也证明了该模型在 AZ61镁合金电子束平板焊接的热效应模拟中有较好的适用性.

关键词：镁合金；电子束焊接；复合热源；焊缝成形；数值模拟
中图分类号：TG156　文献标识码：A　文章编号：0253－360X（2010）06－0065－04

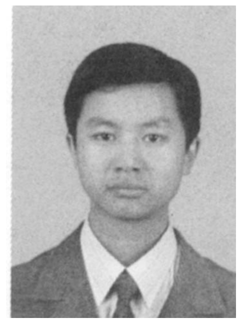

罗　怡

0　序　　言

镁合金是目前工业应用最轻的金属结构材料之一，但其熔点低、导热率高、线膨胀系数大、表面张力小、化学活性大，使镁合金焊接过程产生一系列的困难，如合金元素的氧化与蒸发，组织过热，焊接后易出现气孔等问题. 电子束是一种具有极高功率密度的焊接热源，利用加速电子束流高速轰击材料表面，产生高温熔化效应，形成钉状焊缝，从而获得深熔焊接效果，可用于多种工程材料的高速焊接. 在用于镁合金材料焊接中，真空环境为镁合金提供了理想的加工空间，在纯镁、AZ31、AZ61、AZ91等材料均已取得了较为理想的效果[1－4].

为了深入研究真空电子束焊接热效应，各种不同的热源模型被提出，以用于热效应的数值模拟研究，如圆锥形体热源模型、分段移动双椭球热源模型、旋转高斯曲面体热源模型等[5－7]. 这些热源模型较为充分地考虑了电子束热源深熔焊接的效果，实现了电子束焊接温度场的数值模拟. 在镁合金的真空电子束焊接过程中，由于镁合金中 Mg, Zn等元素沸点低，在高功率密度的热源作用下伴随强烈的蒸发现象，形成高温金属蒸气等离子体，产生特殊的“匙孔”效应，从而得到大深宽比的“钉”状焊缝. 为了在镁合金真空电子束焊接热效应数值模拟研究中充分考虑上述物理效应，在此研究中建立了高斯面热源和双椭球体热源复合的热源模型，实现了电子束热源焊接镁合金板材的温度场模拟，并以此研究焊缝成形预测，为进一步深入研究镁合金真空电子束焊接机理奠定了基础.

1　焊接温度场计算模型

1.1　基本假设

电子束焊接过程中，影响传热的因素较多，包括材料热物理参数在内的非线性因素导致求解过程收敛困难. 因此，在模拟过程中有必要对某些因素进行简化或假设处理，特作以下近似假设. （1）试件初始温度为室温 20 ℃；（2）忽略电子束对熔池的搅拌作用及熔池内的气液相对流、化学反应等现象；（3）假设熔池表面为平面，忽略电子束热源对熔池表面形态的影响；（4）焊接过程恒速进行，热源能量密度分布符合建立的理想模型.

1.2　焊接试板模型

焊接采用的试板材料为 AZ61镁合金，其尺寸如图 1所示. 基于试板尺寸，建立物理模型时考虑对称几何形状的二分之一焊缝模型. 焊接过程是个不均匀的加热过程，不同区域温度梯度的变化很大，因此模型的网格划分是不均匀的. 根据数值模拟的

收稿日期：2009－01－05
基金项目：江苏科技大学先进焊接技术省级重点实验室开放研究基金资助项目

需要,焊缝区采用 8节点六面体单元,网格划分较细,计算精度较高;远离焊缝区能量传递缓慢,温度梯度变化相对较小,采用稀疏单元网格;焊缝区与远离焊缝区之间的过渡区采用 10节点四面体单元,在保证计算精度的前提下,减少网格数量. 焊缝模型的网格划分如图 2所示.

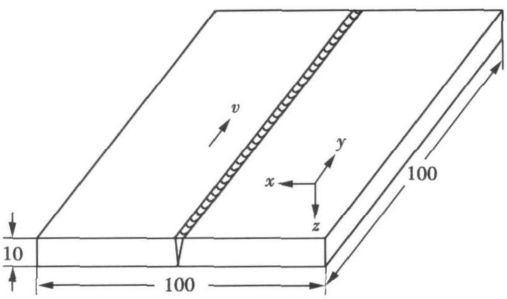

图 1 焊接试板示意图(mm)
Fig. 1 Schematic of test piece for welding

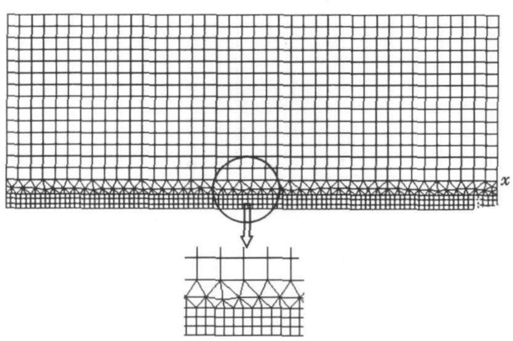

图 2 焊缝模型网格划分
Fig. 2 Mesh of weld model

对于焊接过程,焊接区材料随时间变化经历不同温度区间,计算结果与变化过程密切相关. 由于AZ61镁合金高温热物理参数并不齐全,因而未知温度处的参数可以通过插值法和外推法来确定. 这对于计算结果精确度有一定影响.

1.3 热源模型

焊接热源具有移动的特点,而电子束焊接属于深熔焊接,热源具有极高的功率密度,在高温金属蒸气反作用力作用下,冲击效应较大,形成"匙孔"效应,易得到深熔焊接效果. 这种热效应可以采用三维移动双椭球体热源模拟. 另一方面,镁合金中低沸点金属元素在高功率密度热源的作用下,容易蒸发. 在真空焊接环境下,"匙孔"内充满高温金属蒸气,与外部空间形成较大的压力梯度,不断从"匙孔"中喷出,从而在"匙孔"表面形成高温金属蒸气等离子体,其热效应使真空电子束焊缝形成较大的开口,即"钉"状焊缝. 这就是大深宽比焊缝的形成机制. 考虑到这种能量分布规律,"匙孔"表面金属蒸气等离子的热效应采用移动高斯面热源来模拟. 即建立高斯面热源与双椭球体热源复合的热源模型来实现镁合金的真空电子束深熔焊接模拟.

对于双椭球体热源,该热源模型由两个 1/4椭球组合而成. 前半部分椭球热源温度梯度陡变,其热流密度分布为

$$q_f(x,y,z)=\frac{6\sqrt{3}f_fQ}{abc_f\pi^{3/2}}\exp\left[-3\left(\frac{x^2}{a^2}+\frac{z^2}{b^2}+\frac{y^2}{c_f^2}\right)\right] \tag{1}$$

后半部分椭球温度梯度变化较缓,其热流密度分布为

$$q_b(x,y,z)=\frac{6\sqrt{3}f_bQ}{abc_b\pi^{3/2}}\exp\left[-3\left(\frac{x^2}{a^2}+\frac{z^2}{b^2}+\frac{y^2}{c_b^2}\right)\right] \tag{2}$$

式中:a, b, c_f, c_b为热源形状参数,可取不同值,且相互独立;f_f, f_b为前后椭球热源能量分配系数;Q为热输入功率,其表达式为

$$Q=CU_aI_b \tag{3}$$

式中:C为电子束热源有效功率系数;U_a为加速电压;I_b为电子束流.

考虑到焊接热源移动的特点,空间中沿焊接速度方向,各处输入热流密度在不断发生变化,经坐标变换,式(1),式(2)分别可表述为

$$q_f(x,y,z)=\frac{6\sqrt{3}f_fQ}{abc_f\pi^{3/2}}\exp\left\{-3\left\{\frac{x^2}{a^2}+\frac{z^2}{b^2}+\frac{[y+v(\tau-t)]^2}{c_f^2}\right\}\right\} \tag{4}$$

$$q_b(x,y,z)=\frac{6\sqrt{3}f_bQ}{abc_b\pi^{3/2}}\exp\left\{-3\left\{\frac{x^2}{a^2}+\frac{z^2}{b^2}+\frac{[y+v(\tau-t)]^2}{c_b^2}\right\}\right\} \tag{5}$$

式中:t为焊接时间;τ为焊接热源的时间延迟因子;v为焊接速度.

对于高斯面热源,其热流密度分布为

$$q_s(x,y)=\frac{3Q}{\pi r_0^2}\exp\left[-\frac{3(x^2+y^2)}{r_0^2}\right] \tag{6}$$

式中:r_0为热源作用半径.

考虑到焊接热源移动的特点,经坐标变换,式(6)可表述为

$$q_s(x,y)=\frac{3Q}{\pi r_0^2}\exp\left\{-\frac{3[x^2+(y+v(\tau-t))^2]}{r_0^2}\right\} \tag{7}$$

2 电子束焊接热效应模拟

加速电压、电子束流、焊接速度等工艺参数对焊

缝成形及其焊接过程的温度场分布有着重要的影响. 将建立的复合热源模型以热流密度的形式作用于试件表面. 由于焊接在真空中进行,焊接过程中不考虑试件与真空环境的对流换热,而仅考虑热辐射. 将试件的初始温度设为与环境温度相同,即室温 20 ℃. 在实体单元表面生成表面效应单元,并施加辐射载荷,以此来考虑边界条件.

图 3为模拟得到的 AZ61镁合金真空电子束焊接温度场分布三维图和热循环曲线图. 采用的焊接工艺参数为:加速电压 60 kV,电子束流 25 mA,焊接速度 18 mm/s. 从图 3a焊接方向上的前后温度梯度分布差异可以看出,模拟过程很好地再现了移动热源对焊缝金属的加热特点,焊接方向的熔池前沿由于迅速加热至熔化,温度梯度较大;焊接方向的熔池后沿,加热熔化后的焊缝逐渐凝固冷却,温度梯度分布趋于缓和. 由于施加了高斯面热源模拟高温金属蒸气等离子体的热效应,熔池表面表现出了较大的开口,这与实际的镁合金真空电子束焊接过程的熔池表面形态基本一致. 图 3b中三条热循环曲线分别为焊缝表面距离束斑 0.5, 1.5, 2.5 mm三点的温度变化. 从峰值温度可以看出,三点中, 0.5 mm点位于接近焊缝中心区, 1.5 mm点基本位于焊缝固液界面处, 2.5 mm点位于近缝区. 各点温度梯度变化显著大于普通电弧焊接,这与真空电子束焊接机理密切相关. 普通电弧热源功率密度较低,焊接过程为热传导传热机理,即焊接电弧热通过电弧热传导将焊接能量传递给熔池金属材料,其加热速率相对低于高功率密度的电子束. 真空电子束焊接过程中,功率密度极高的电子束流高速冲击镁合金材料表面,电子束流动能转换成热能并释放,使金属部分合金元素迅速熔化、蒸发,产生金属蒸气,而金属合金元素蒸发过程中产生的金属蒸气反作用力排开液态熔融金属,使电子束直接作用于熔池底部,从而产生大深宽比“钉”状焊缝. 这种焊缝特征在图 4中的焊缝横截面等温线图中得到体现. 为了更好表现电子束热源作用下的镁合金焊缝成形特征,下文研究了不同焊接工艺参数下的电子束焊缝成形特点.

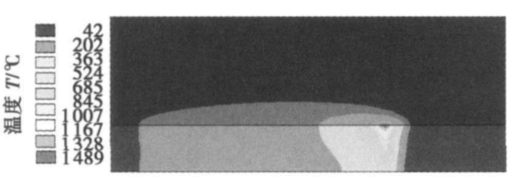

(a) 焊缝温度场分布三维图

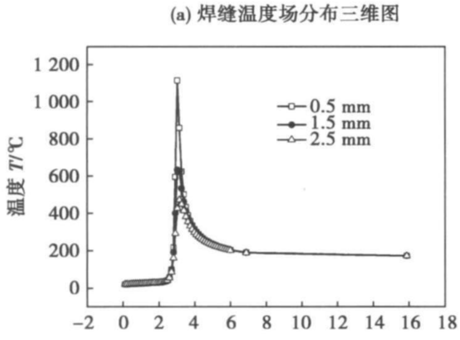

(b)焊缝热循环曲线

图 3　电子束流 25 mA的焊缝温度场分布

Fig. 3　Distribution of weld temperature field at welding beam current of 25 mA

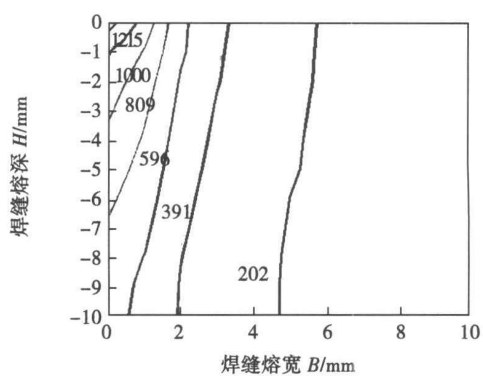

图 4　焊缝横截面等温线

Fig. 4　Isotherm in cross-section of weld bead

3　焊缝成形模拟

选择三组焊接工艺参数对 10 mm厚 AZ61镁合金试板进行焊接试验,如表 1所示. 真空条件为 5×10^{-2} Pa. 焊前用丙酮清洗试样去除油污,干燥后用砂纸进行接口处清理以去除氧化膜. 根据温度场的模拟数据,选择焊缝某一截面,经计算分别得到三条焊缝横截面的二分之一形貌特征. 图 5为镁合金真空电子束焊接试验焊缝形貌与计算所得焊缝形貌的对比. 图 5a中,焊接选用的热输入较小,为 40 J/mm,试板未穿透,镁合金中金属合金元素的蒸发产生的金属蒸气从“匙孔”开口处喷出,其热效应较为显著,形成典型的“钉”状焊缝. 由于以高斯面热源的形式考虑了金属蒸气等离子体的热效应,可以

表 1　焊接工艺参数

Table 1　Welding parameters

编号	电子束流 I_b/mA	加速电压 U_a/kV	焊接速度 $v/(mm\cdot s^{-1})$	热输入 $E/(J\cdot mm^{-1})$
1	20	60	30	40.0
2	25	60	18	83.3
3	35	60	18	116.7

看出计算得到的焊缝形貌较为准确地反映了试验焊缝形貌特征．图 5b中，采用的焊接热输入为 83.3 J/mm，焊缝刚好熔透，从试验焊缝形貌和计算得到的焊缝形貌可以看出，二者是比较吻合的．图 5c中，采用的焊接热输入已完全熔透焊缝，相当部分的高温金属蒸气从熔透的焊缝底部排出，减弱了金属蒸气等离子体在焊缝表面开口处的热效应，因此，从计算结果及试验焊缝均可看出，两条焊缝熔合线近乎平直．

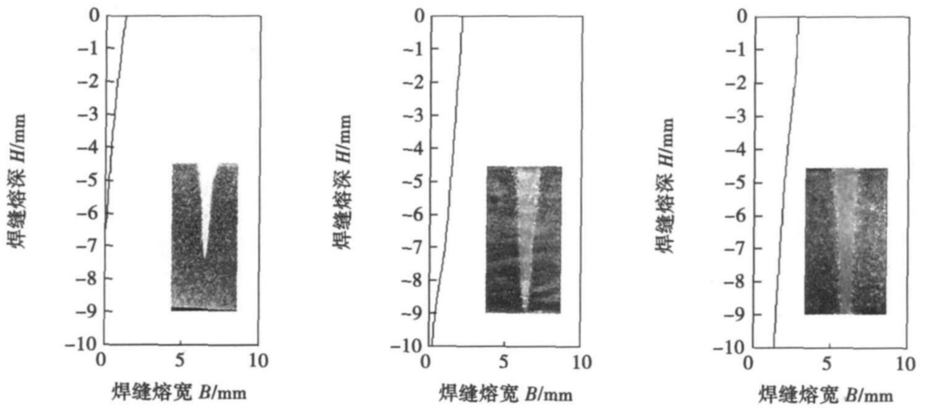

(a) 热输入E = 40.0 J/mm　(b) 热输入E = 83.3 J/mm　(c) 热输入E = 116.7 J/mm

图 5　焊缝形貌的计算值与试验值对比

Fig. 5　Comparison of calculated value and measured value for weld bead

4 结　　论

（1）高斯面热源与双椭球体热源复合的真空电子束焊接热源模型合理地模拟了镁合金的真空电子束深熔焊接的热效应特征．

（2）计算得到的焊缝形貌特征与真空电子束焊接试验焊缝成形基本吻合，证明了建立的热源模型在利用热效应计算焊缝形貌特征中的适用性．

参考文献：

[1] Toshikarsu Asahina, Hiroshi Tokisue. Electron beam weldability of pure magnesium and AZ31 magnesium alloy[J]. Journal of Japan Insititute of Light Materials, 2002, 50(10): 512－517.

[2] Munitz A, Cotler C. Electron beam welding of magnesium AZ91D plates[J]. Welding Journal, 2000, 79(7): 202s－208s.

[3] Su S F, Huang J C, Lin H K, et al. Electron beam welding behavior in Mg-Al-based alloys[J]. Metallurgical Materials Transactions, 2002, 33A: 1461－1464.

[4] Asahina T, Ohkubo M. Mechanical properties of electron beam welded joints of AZ80 magnesium alloy[J]. Journal of Japan Insititute of Light Materials, 1994, 44(4): 210－215.

[5] 胡美娟，刘金和，王亚军，等．钛合金平板电子束焊接温度场有限元分析[J]．电焊机，2005，35(7)：39－42.
Hu Meijuan, Liu Jinhe, Wang Yajun, et al. Finite element analysis of temperature field in electron beam welding of titanium plate[J]. Electric Welding Machine, 2005, 35(7): 39－42.

[6] 王　煜，赵海燕，蔡志鹏，等．电子束焊接数值模拟中分段移动双椭球热源模型的建立[J]．机械工程学报，2004，40(2)：165－169.
Wang Yu, Zhao Haiyan, Cai Zhipeng, et al. Establishment of segmented moving double ellipsoid heat source model in electron beam welding numerical simulation[J]. Chinese Journal of Mechanical Engineering, 2004, 40(2): 165－169.

[7] 王西昌，吴　冰，左从进，等．电子束焊接数值模拟新型热源模型的初步探索[J]．焊接学报，2005，26(12)：81－84.
Wang Xichang, Wu Bing, Zuo Congjin, et al. New heat source model for numerical simulation of electron beam welding[J]. Transactions of the China Welding Institution, 2005, 26(12): 81－84.

作者简介：罗　怡，男，1979年出生，博士研究生，讲师．主要研究方向为焊接方法及自动化．发表论文 20余篇．
Email: luoyi@cqut.edu.cn

surface, which the boiler withstands the supercritical pressure and the ultra 570 ℃ high temperature in manufacture and installment first-phase 2×600 MW coal-fired generating units in China-HK (Hong Kong) joint project through the Zhuhai Power plant. The metal characteristics and welding performance of the two kind steels are analyzed, and the primary factors of producing crack, corrosion and embrittlement flaw in the boiler production and the movement process are determined by experiments, and the craft evaluation of the parent metal and the welding material has carried out by using the corresponding craft measure. The fine weld joints are obtained, which will promote the using of the T91 and TP347H heat-resistant steel in the manufacture of the promotion (ultra) supercritical pressure thermal power unit boiler.

Key words: critical; T91; TP347H; heterogenic-steel weld

Effect of thermophysical parameters on the hump feature of welding residual stress by finite element analysis

YAN Dejun, LIU Xuesong, YANG Jianguo, FANG Hongyuan (State Key Laboratory of Advanced Welding Production Technology, Harbin Institute of Technology, Harbin 150001, China). p 56－60

Abstract: Numerical simulation of TIG welding of thin plate by thermo-elastic finite element method (FEM) was conducted. By double ellipsoid thermal source, thermophysical parameters varying with temperature were used to compare the influence of heat conductivity, specific heat capacity and density on the welding residual stress. The result shows that the drop of the heat conductivity will lead to the increment of the welding residual stress, and the longitudinal residual stress transits from the double hump to the single one; the falling of the specific heat capacity can also reduce the welding residual stress, which can greatly be affected by the difference of density between aluminum alloy and mild steel, and the double hump of the longitudinal residual stress will disappear with the density increasing. Then the three thermo-physical parameters, heat conductivity, specific heat capacity and density, make the longitudinal welding residual stress of aluminum alloy is lower than its yield limit and appears double hump effect near the weld seal. The welding longitudinal residual stress for the flat plates of 2024-T4 aluminum alloy is simulated by using cutting pieces stress relieving method. The simulation results are well accordant with the test ones, which prove the validity of the simulation results.

Key words: numerical simulation; longitudinal residual stress; thermophysical parameters; double hump effect

Establishment of relation about welding residual stress between simulative component and practical component on basis of similitude principles

JI Shude[1], ZHANG Liguo[1], LI Yafan[2], LIU Xuesong[2], FANG Hongyuan[2] (1. School of Aerospace Engineering, Shenyang Institute of Aeronautical Engineering, Shenyang 110034, China; 2. State Key Laboratory of Advanced Welding Production Technology, Harbin Institute of Technology, Harbin 150001, China). p 61－64

Abstract: On basis of the similitude principles, the conception of virtual simulative component and the auxiliary value of welding residual stress are deduced by the welding conduction theory, and the relation of the welding residual stress between the simulative component and the practical component is attained. Moreover, the welding experiment about the simulative plane and the practical plane proves the correctness of the relation, which the proportionality coefficient of dimensions between the simulative plane and practical plane is 1∶1.5. This provides a new idea to predict the welding stress distribution of large practical structure by the contractible physical model and has owns important theory meaning and practical engineering significance.

Key words: similitude principles; conduction theory; simulative component; welding residual stress

Numerical simulation on electron beam deep penetration welding and weld appearance of magnesium alloy

LUO Yi[1,2,3], LIU Jinhe[1], YE Hong[3], SHEN Bin[3] (1. School of Material Science and Engineering, Northwestern Polytechnical University, Xi'an 710072, China; 2. Province Key Laboratory of Advanced Welding Technology, Jiangsu University of Science and Technology, Zhenjiang 212003, Jiangsu, China; 3. School of Material Science and Engineering, Chongqing Institute of Technology, Chongqing 400050, China). p 65－68

Abstract: The numerical simulation on vacuum electron beam deep penetration welding for AZ61 magnesium alloy sheet with 10 mm thickness was studied. In view of the thermal effect about metal steam plasma and keyhole deep penetration during vacuum electron beam welding, the moving heat source model composed by Gauss surface source and double ellipsoid body source was developed. And the characteristics of thermal cycle and weld appearance under different welding processes were studied on the basis of simulation and experiment values. The results of simulation and experiment show that the composite source model can gain the effect of deep penetration of electron beam welding and calculate the temperature distribution and the weld geometry under the action of electron beam source. The results also prove that the model is applicable to the thermal effect simulation on the electron beam welding of AZ61 magnesium alloy sheet.

Key words: magnesium alloy; electron beam welding; composite heat source; weld appearance; numerical simulation

Effect of heat input on microstructure and low temperature impact resistance of welded joint of 9Ni steel

Menggenbagen[1,2], MA Chengyong[2], PENG Yun[2], TIAN Zhiling[2], LIN Wenguang[1] (1. College of Materials Science and Engineering, Inner Mongolia University of Technology, Huhhot 010051, China; 2. Central Iron & Steel Research Institute, Beijing 100081, China). p 69－72

Abstract: 9Ni steel was welded with submerged arc welding process, and the microstructure and fracture appearance of welded joints were analyzed. The effect of heat input on the microstructure and low temperature impact resistance of the joints was studied. The results show that with the increase of the heat input, dendritic segregation and precipitation phase in the weld reduce, and fracture dimples become larger and deeper, which make the impact resistance of the joints increase. The joints in different input can meet application requirements, which impact absorbing energy is superior to standard at -196 ℃ and hardness is inferior to 400 HV. The experiment results can be used as theoretic basis for making welding procedure of 9Ni steel.

Key words: 9Ni steel; heat input; welded joint; micro-